International Journal of Thermal Sciences 96 (2015) 12–22

Contents lists available at ScienceDirect

International Journal of Thermal Sciences

journal homepage: www.elsevier.com/locate/ijts

Heat generation and conduction in PDMS-carbon nanoparticle membranes irradiated with optical fibers

J. Rodrigo Vélez-Cordero [a, *], Juan Hernández-Cordero [b]

[a] Instituto de Física "Manuel Sandoval Vallarta", Universidad Autónoma de San Luis Potosí, Alvaro Obregón 64, 78000 San Luis Potosí, S.L.P., Mexico
[b] Instituto de Investigaciones en Materiales, Universidad Nacional Autónoma de México, Apdo. Postal 70-360 México D.F. 04510, Mexico

ARTICLE INFO

Article history:
Received 13 June 2014
Received in revised form
13 April 2015
Accepted 15 April 2015
Available online 22 May 2015

Keywords:
Polymer
Composites
Carbon
Nanoparticles
Optical
Fibers
Heat
Conduction

ABSTRACT

Carbon based materials have recently been used to fabricate highly photo-absorbing surfaces for heat generation purposes. In this report we present experimental measurements of the temperature increments ΔT in polymer (PDMS)-carbon nanopowder membranes irradiated by a light source via an optical fiber. In particular, we analyze experimentally the effects of the optical depth, $\tau_\lambda = \beta L$, on the transient and steady state temperature profiles. In order to analyze the experimental data under the heat conduction theory, we also constructed a 2D axi-symmetric heat transfer solution for a semi-transparent finite membrane using Green's functions. With this approach we obtained two analytical expressions: one for the axial unsteady profile and another for the steady ΔT profile in the $r-z$ plane using the delta function approximation. We found a linear relationship between the experimental ΔT steady values and the optical intensity I_o; this linear relationship was maintained until incandescence at the membrane surface appeared. We also found that the steady ΔT values had little dependance on the membrane thickness L; conversely, the transient ΔT values exhibited a clear dependance on L, as expected. The theoretical solution fitted the experimental data only for a thermal diffusivity smaller than that of pristine PDMS. Our analysis suggests that such heat transfer retardation may be due to the nonlinear scattering behavior of the composite or due to additional interfacial resistances imposed by the experiment. Finally, experiments and theory showed that the $L-\Delta T$ curves have a maximum point (maximum temperature) at an optimal membrane thickness L_{op}; this optimal point in turn decreases as the extinction coefficient increases. Additional analysis of the results were also conducted regarding the area of the membranes, and both, experiments and theory, suggest that the heat generation induced by irradiating a surface with optical fibers is indeed highly localized.

1. Introduction

It is surprising that carbon, one of the main constituents of life, has been considered a promising material to construct non-organic devices due to its fascinating electronic, thermal and optical properties [1–4]. Inherent to graphene-like allotropes, two convenient properties of carbon molecules arise thanks to its chemical structure signature. The sp^2 hybridization in the graphene lattices (conjugated single and double bonds) facilitate the excitation of electrons by light irradiation, making graphene a non-transparent material – black – for a wide range of the electromagnetic spectrum [2,5]. The energy absorbed by the electrons relaxes by means of electron-phonon couplings [6–8], avoiding the re-emission of photons at low temperatures. Hence, carbon allotropes not only absorb light but also transfer the energy of the excited electrons to vibrational modes within the atomic lattices, macroscopically rising the temperature of the material. In pure carbon nanotubes, for example, where the recurrence of atomic defects is practically absent, the transmission of the molecular vibration is very efficient (large phonon mean free paths), providing these materials with very good thermal conductivities [4].

The properties of carbon allotropes mentioned so far have encouraged researchers to investigate the applications of carbon nanoparticles as heat deliverers; recent research fronts contemplate, for example, the use of carbon nanotubes for photothermal cancer treatment [9], light absorption and combustion in polymer-carbon composites to produce high-resolution micropatterns [10], and light absorption in composites to induce thermocapillary

* Corresponding author.
E-mail address: jrvelez@ifisica.uaslp.mx (J.R. Vélez-Cordero).

http://dx.doi.org/10.1016/j.ijthermalsci.2015.04.009
1290-0729/

Nomenclature

$A=w^2/2$	beam size parameter
a	membrane area
$Bi=HL$	Biot number
h	heat transfer coefficient
$H=h/k$	convection to conduction ratio
I_o	optical intensity
k	thermal conductivity
L	membrane thickness
P_o	optical power
$q(x),q(r,z)$	heat generation term
t	time
w	laser beam radius
x	1D space coordinate
r,z	2D axi-symmetric space coordinates

Greek symbols

α	thermal diffusivity
β	extinction coefficient
λ_n	eigenvalues of the finite space solution
$\theta=\Delta T=T-T_o$	temperature increment
τ	instantaneous time in the Green's function
$\tau_\lambda=\beta L$	optical depth

subscripts

1,2	front and back surfaces of the membrane
op	optimum value
abs	absorption term
scat	scattering term
o	temperature or optical intensity reference value

pumping in micro-channels [11]. Among other interesting physical phenomena [12], the thermal properties of polymer-carbon composites have been particularly studied due to the fact that pure carbon nanoparticle blocks are not mechanically stable and have large porosities: this is the reason why it is a common practice to mix nanoparticles with a secondary phase [13]. At first, it was thought that mixing a high thermal conductivity material, such as carbon nanoparticles, with another material having low thermal conductivity, such as polymers, would rise the heat conductivity of the overall composite according to the mixing model [13]. Different reports have shown that this is actually not the case due to the different phonon spectra between phases, highlighting the importance of considering an interfacial resistance [13–15]. As a rule of thumb, it is necessary to add ~10% v/v of carbon nanoparticles in order to triple the amount of thermal conductivity in the composite, although recently, highly packed carbon nanotubes have shown to double the conductivity in composites with just 1% [16].

Another interesting behavior that has been observed in polymer-carbon composites or carbon nanofluids is the optical limiting behavior associated with nonlinear scattering mechanisms [17–19]. When photo-absorption rises the temperature of the composite, bubbles or carbon microplasma can be formed in the media which in turn act as scattering centers. Therefore, the light transmitted through the composite seems to decrease in a nonlinear fashion as the optical power increases. This behavior has been actually used in optical devices in order to impose a light transmission limit and guarantee power-dependant light screening [17].

The main objective of the present investigation is to measure experimentally the temperature rise in polymer-carbon membranes irradiated by light. Special attention is given to the effect that the membrane thickness has on the steady and transient temperature states, as well as in the effects of the optical intensity and associated nonlinear scattering mechanisms. Temperature measurements in photo-irradiated slabs have been conducted in the past mainly with metals, glass, silica or other non-metallic materials [20–23], but less work has been done in the case of polymer-carbon membranes (with thicknesses well above the mean free path of the energy carriers). Composites of this nature can be used as microheaters in microfluidic devices or MEMS, hence the interest in characterizing their heat transfer characteristics. In order to correlate the experimental results with the thermal properties of the composite, we developed a two-dimensional (2D) axi-symmetric model and emphasized in the obtention of analytical solutions to avoid the use of numerical algorithms. After introducing the mathematical model in the next section, we describe the experimental setup in section 3, including the temperature and optical transmittance measurements of the membranes. Next, the results are presented in section 4 followed by a comparison between the experimental and theoretical results in section 5. The effects of the extinction coefficient and membrane thickness in the temperature increment is then discussed followed by a description of the radial and steady-state 2D temperature profiles estimated with the analytical equations. Some conclusions are finally outlined in section 6.

2. Mathematical model

The mathematical model decouples the global energy equation and the radiative heat equation. This simplification arises from two principal considerations: the experiments are conducted at room temperature (negligible emission), and thermal diffusion is more affected by absorption than by scattering (light excitation wavelength falls in the range that yields maximum absorption). Note that these two main considerations may fail at large optical powers since under these conditions both, emission and/or scattering effects are likely to play a more significant role. As a note, it is worth noticing that scattering may lead to a decrease in the apparent thermal diffusivity, although it seems to have no effects under steady state conditions, as suggested by Refs. [22,24]. The equations obtained in this section may be added to the family of equations and numerical algorithms relating similar problems, which can be found in, among others: pure conduction in semi-infinite non-transparent materials [25,26], conduction/emission in semi-infinite non-transparent materials [21], pure conduction in semi-infinite semi-transparent materials [27], conduction/scattering in finite semi-transparent materials [28–30], conduction/scattering/emission (with and without external convection) in semi-infinite slabs or layered composites [22,24].

Consider then a composite membrane (mixture of polymer and carbon nanoparticles) having a thickness L (Fig. 1). At the two surfaces or boundaries, heat can be dissipated by the surrounding media characterized by two heat transfer coefficients. The generation term q in the heat transfer equation is given by the gradient of the Beer–Lambert law. In what follows, we are going to show the 1D and 2D axi-symmetric solutions for the present problem and later compare them using representative values of the thermal characteristics of the composite. Note that the 1D solution is only

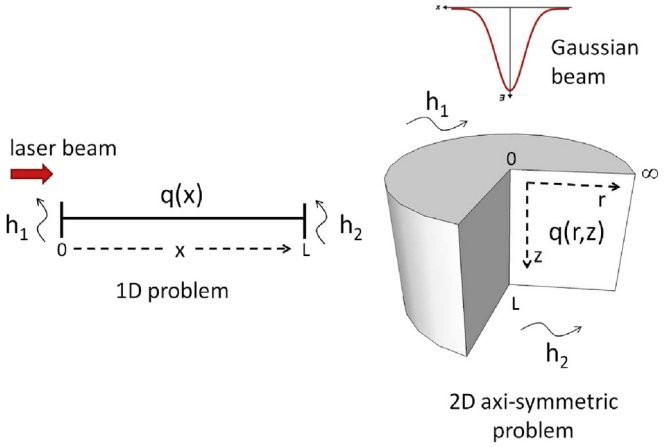

Fig. 1. Schematic representation of the 1D and 2D axi-symmetric heat problems used in the mathematical formulation. L is the membrane thickness, $q(x)$, $q(r,z)$ are the heat generation terms, and h_1, h_2 are the heat transfer coefficients on the front and back surfaces, respectively.

applicable when planar wave fronts are considered, while the 2D solution is more general in the sense that it can include wavefronts of different shapes or finiteness.

2.1. 1D solution

The 1D global heat equation, using the variable $\theta=\Delta T=T-T_o$, can be written as:

$$\frac{\partial^2\theta}{\partial x^2}+\frac{q(x)}{k}=\frac{1}{\alpha}\frac{\partial\theta}{\partial t}, \tag{1}$$

where the heat generation term $q(x)$ is obtained from the radiative heat equation considering negligible scattering and emission [31], i.e.:

$$q(x)=\beta I_0 e^{-\beta x}. \tag{2}$$

In the present problem, the homogeneous boundary and initial conditions are:

$$-k\frac{\partial\theta}{\partial x}\bigg|_{x=0}=-h_1\theta|_{x=0},\quad -k\frac{\partial\theta}{\partial x}\bigg|_{x=L}=h_2\theta|_{x=L},\quad \theta(x,t=0)=0. \tag{3}$$

Solution of the 1D problem can be obtained by standard methods (separation of variables, eigenfunction expansions) using the superposition principle [32]. The temperature evolution is then represented as a sum of steady and transient terms $\theta(x,t)=\theta_s(x)+\theta_H(x,t)$, where the generation term is linked to the steady solution $\theta_s(x)$ and the transient part is coupled to the steady one using the modified initial boundary condition $\theta_H(x,t=0)=-\theta_s$. The solution for the 1D heat conduction problem is then obtained as:

$$\theta(x,t)=-C_1x+C_2-\frac{I_o}{\beta k}e^{-\beta x}+2\sum_{n=1}^{\infty}e^{-\alpha\lambda_n^2 t}\frac{I_1(\lambda_n)}{N(\lambda_n)}[\lambda_n\cos(\lambda_n x)+H_1\sin(\lambda_n x)], \tag{4}$$

where

$$C_1=\frac{I_0\left[e^{-\beta L}\left(\frac{h_1}{h_2}-\frac{H_1}{\beta}\right)+\left(\frac{H_1}{\beta}+1\right)\right]}{k\left(1+\frac{h_1}{h_2}\right)+h_1L}, \tag{5}$$

$$C_2=\frac{I_o}{h_2[k(1+h_1/h_2)+h_1L]}\left[-e^{-\beta L}\left(k-\frac{h_2}{\beta}\right)+\frac{h_1}{\beta}+\frac{h_1h_2L}{\beta k}+h_2L+k\right], \tag{6}$$

$$N(\lambda_n)=\left(\lambda_n^2+H_1^2\right)\left(L+\frac{H_2}{\lambda_n^2+H_2^2}\right)+H_1, \tag{7}$$

$$\begin{aligned}I_1(\lambda_n)=&\frac{1}{\lambda_n}\left[\frac{\sin(\lambda_nL)}{\lambda_n}\left(C_1\left(\lambda_n^2L+H_1\right)-\lambda_n^2C_2\right)\right]\\&+\frac{1}{\lambda_n}[\cos(\lambda_nL)\{C_1(1-H_1L)+C_2H_1\}-C_1-C_2H_1]\\&+\frac{I_o\lambda_n}{k\left(\beta^2+\lambda_n^2\right)}\left[1-\cos(\lambda_nL)e^{-\beta L}+\frac{\lambda_n}{\beta}\sin(\lambda_nL)e^{-\beta L}\right]\\&+\frac{I_oH_1}{k\left(\beta^2+\lambda_n^2\right)}\left[\frac{\lambda_n}{\beta}-\frac{\lambda_n}{\beta}\cos(\lambda_nL)e^{-\beta L}-\sin(\lambda_nL)e^{-\beta L}\right],\end{aligned} \tag{8}$$

and the values of $\lambda_n=\eta_n/L$ are given by the transcendental function:

$$\tan(\eta_n)=\frac{\eta_n(Bi_1+Bi_2)}{\eta_n^2-Bi_1Bi_2}\quad\text{for}\quad n=1,2,3\ldots \tag{9}$$

In the equations above, $H_{1,2}=h_{1,2}/k$ is the ratio between the heat transfer coefficient and the thermal conductivity, and $Bi_{1,2}=H_{1,2}L$ is the Biot number. In the limit $\beta\to\infty$, Eq. (4) reduces to the finite 1D solution in which the optical intensity is fully absorbed at the surface, i.e., opaque materials.

2.2. 2D axi-symmetric solution

The temperature evolution in a membrane can be represented in cylindrical coordinates by a semi-infinite domain ($0\le r\le\infty$, $0\le z\le L$, see Fig. 1), having no variation of the temperature in the azimuthal direction. The global heat equation is then written as:

$$\frac{1}{r}\frac{\partial}{\partial r}\left(r\frac{\partial\theta}{\partial r}\right)+\frac{\partial^2\theta}{\partial z^2}+\frac{q(r,z)}{k}=\frac{1}{\alpha}\frac{\partial\theta}{\partial t}. \tag{10}$$

Let us assume that an unfocused TEM_{oo} laser beam induces a generation term inside the material having a Gaussian profile

$$q(r,z)=\beta I_o e^{-\beta z-r^2/A}, \tag{11}$$

where $A=w^2/2$ and w is the laser beam radius at which the optical intensity $I_o=P_o/A\pi$ decays to e^{-2}. In doing this we are indeed assuming that the rays trajectories are not altered by scattering and that the membrane thickness L is too small to consider beam divergence. As in the 1D solution, the boundary and initial conditions are homogeneous:

$$-k\frac{\partial\theta}{\partial z}\bigg|_{z=0}=-h_1\theta|_{z=0},\quad -k\frac{\partial\theta}{\partial z}\bigg|_{z=L}=h_2\theta|_{z=L},\quad \theta(r,z,t=0)=0. \tag{12}$$

Eq. (10) cannot be solved using the superposition principle due to the dependance of the generation term on the spatial coordinates. The solution of this problem can be obtained, however, invoking the auxiliary problem [32,33]:

$$\frac{1}{r}\frac{\partial}{\partial r}\left(r\frac{\partial \mathscr{G}}{\partial r}\right)+\frac{\partial^2 \mathscr{G}}{\partial z^2}+\frac{1}{k}\delta(r-r')\delta(z-z')\delta(t-\tau)=\frac{1}{\alpha}\frac{\partial \mathscr{G}}{\partial t}, \tag{13}$$

where $\mathscr{G}$ is the Green's solution for a heat source located at (r', z') and turned on instantaneously at time τ. The temperature profile in the whole domain can then be recovered by the integral transform:

$$\theta(r,z,t)=\frac{\alpha\beta I_o}{k}\int_{\tau=0}^{t}\int_{0}^{\infty}\int_{0}^{L}\mathscr{G}(r,z,t|r',z',\tau)e^{-\beta z'-r'^2/A}r'dz'dr'd\tau, \tag{14}$$

where the notation for the Green's function denotes that the multidimensional Green's solution in axi-symmetric cylindrical coordinates can be obtained by multiplying the individual 1D Green's functions for the r and z spatial coordinates. The multidimensional Green's functions for a variety of spatial domain combinations have been listed by Hahn & Ožişik [32]; for the semi-infinite domain considered here ($0\le r\le\infty$, $0\le z\le L$), the Green's function is given by:

$$\mathscr{G}(r,z,t|r',z',\tau)=\frac{1}{2\alpha(t-\tau)}exp\left[-\frac{r^2+r'^2}{4\alpha(t-\tau)}\right]\mathscr{I}_o\left[\frac{rr'}{2\alpha(t-\tau)}\right]\times 2 \times\sum_{n=1}^{\infty}\frac{e^{-\alpha\lambda_n^2(t-\tau)}}{N(\lambda_n)}\{\lambda_n\cos(\lambda_n z)+H_1\sin(\lambda_n z)\} \times\{\lambda_n\cos(\lambda_n z')+H_1\sin(\lambda_n z')\}, \tag{15}$$

where $\mathscr{I}_0$ denotes the modified Bessel function of the first kind and λ_n are given by Eq. (9). The z'-terms in Eq. (14) can be integrated by applying integration by parts twice. In the particular case of solving the temperature generated at the axis $r=0$, the r'-components in Eq. (14) are easily integrated, yielding:

$$\theta(r=0,z,t)=\frac{A\beta I_o}{2k}\sum_{n=1}^{\infty}\frac{I_2(\lambda_n)}{N(\lambda_n)}[\lambda_n\cos(\lambda_n z)+H_1\sin(\lambda_n z)]\int_0^t\frac{e^{-\alpha\lambda_n^2(t-\tau)}}{(t-\tau)+A/4\alpha}d\tau, \tag{16}$$

where

$$I_2(\lambda_n)=\frac{1}{\beta^2+\lambda_n^2}\left[\lambda_n(\beta+H_1)+e^{-\beta L}\left\{\sin(\lambda_n L)\left(\lambda_n^2-H_1\beta\right)-\lambda_n\cos(\lambda_n L)(\beta+H_1)\right\}\right]. \tag{17}$$

Finally, for a given value of t, the integral with respect to τ can be expressed in terms of the incomplete Gamma function or the exponential integral Ei [34]:

$$\theta(z,t)_{axis}=\theta(r=0,z,t)=\frac{A\beta I_o}{2k}\sum_{n=1}^{\infty}\frac{I_2(\lambda_n)}{N(\lambda_n)}[\lambda_n\cos(\lambda_n z)+H_1\sin(\lambda_n z)]\times e^{\lambda_n^2 A/4}\left[Ei\left(-\alpha\lambda_n^2 t-A\lambda_n^2/4\right)-Ei\left(-A\lambda_n^2/4\right)\right]. \tag{18}$$

Eq. (18) will be our first working equation and represents the temperature increment at the beam axis. As obtained in the 1D problem, the temperature increment $\theta=\Delta T$ is a linear function of the optical intensity I_o. Note, however, that the 2D axi-symmetric solution is explicitly dependent on the total power delivered, $AI_o\approx P_o$, accounting for the finite width of the laser beam.

2.3. . 2D axi-symmetric solution: the delta function approximation

For a small laser spot radius w, as the one delivered by optical fibers, it seems plausible to approximate the Gaussian beam profile as a delta function, with a power peak at $r=0$. In polar coordinates, the delta function can be defined as:

$$\frac{P_o\delta(r)}{2\pi r}=lim_{\frac{1}{A}\to\infty}\frac{P_o}{A\pi}e^{-r^2/A}. \tag{19}$$

Using this definition in Eq. (14) yields:

$$\theta(r,z,t)=\left(\frac{A\beta I_o}{2k}\int_0^t\int_0^\infty\frac{\delta(r')}{(t-\tau)}exp\left[-\frac{r^2+r'^2}{4\alpha(t-\tau)}\right]\mathscr{I}_o\left[\frac{rr'}{2\alpha(t-\tau)}\right]dr'd\tau\right)\times z,\tau-terms \tag{20}$$

After integrating the r'-terms in Eq. (20) using the properties of the delta function, we get:

$$\theta(r,z,t)=\frac{A\beta I_o}{2k}\sum_{n=1}^{\infty}\frac{I_2(\lambda_n)}{N(\lambda_n)}[\lambda_n\cos(\lambda_n z)+H_1\sin(\lambda_n z)]\int_0^t\frac{e^{-\alpha\lambda_n^2(t-\tau)}}{(t-\tau)}exp\left[-\frac{r^2}{4\alpha(t-\tau)}\right]d\tau \tag{21}$$

This integral has analytical solution only when $t\to\infty$ [34], i.e., the steady-state solution. Therefore, the 2D axi-symmetric steady solution is given by:

$$\theta(r,z)_{steady}=\frac{A\beta I_o}{k}\sum_{n=1}^{\infty}\frac{I_2(\lambda_n)}{N(\lambda_n)}[\lambda_n\cos(\lambda_n z)+H_1\sin(\lambda_n z)]\mathscr{K}_o(r\lambda_n)\quad for\quad r>0 \tag{22}$$

where $\mathscr{K}_0$ denotes the modified Bessel function of the second kind. Eq. (22) is our second working equation. Fig. 2a and b shows the temperature profile in the x or z-direction for the 1D and 2D axi-symmetric problems represented by Eqs. (4) and (18), respectively. The solutions were evaluated up to 19 terms, i.e., $n=19$. All parameters are the same in both cases except that $A=12.5\times10^{-3}\,mm^2$ for the 2D case (this value was taken from the experiments, see below). Both boundaries were considered to be surrounded by air, $h_1=h_2=10\,W/m^2\cdot K$. Evidently, the 2D solution gives lower temperature increments because it considers the total amount of power delivered on the material, which in turn dissipates in the radial and axial directions, while the 1D case

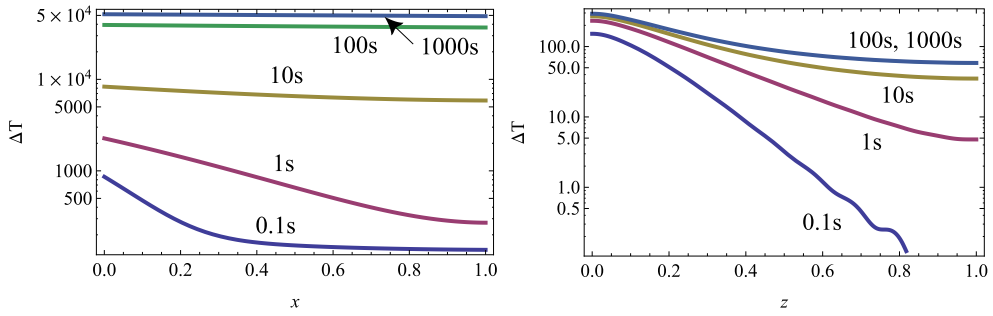

(a) 1D solution (b) 2D axi-symmetric solution

Fig. 2. Theoretical temperature profiles for the 1D an 2D axi-symmetric problems at different times having I_o=1 W/mm^2, $h_1 = h_2 = 10$ W/m^2·K, $k = 0.2$ W/m·K, α=0.1419 mm^2/s, β=10 mm^{-1}, L=1 mm; for the 2D case A=12.5×10^{-3} mm^2. The values of the thermal properties represent typical values for PDMS (poly-dimethylsiloxane).

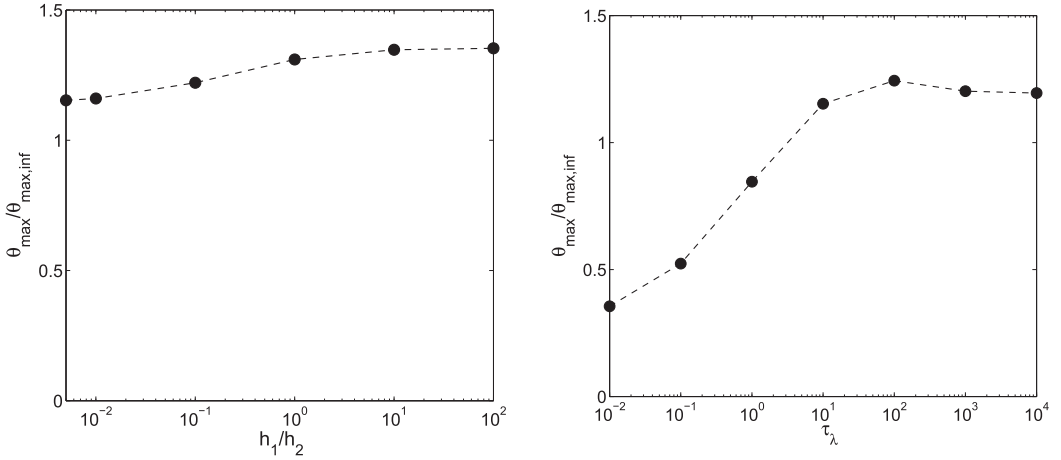

(a) ratios of the maximum temperatures vs h_1/h_2 (b) ratios of the maximum temperatures vs τ_λ

Fig. 3. Comparison of the maximum theoretical steady temperatures θ_{max} reached at (z = 0, r = 0, t = 1000s) computed with Eq. (18) with the one obtained in a semi-infinite slab $\theta_{max,inf}$ (Lax's solution Eq. (23)). a) temperature ratio as a function of the heat transfer coefficient ratio h_1/h_2, b): temperature ratio as a function of the optical depth τ_λ=βL.

assumes that the intensity I_o acts all over the surface (planar wave) and dissipates just in the axial direction. The 2D geometry can give the same temperature increments as the 1D case if one assumes laser beams with larger radius, i.e. as $A \to \infty$ (in the example shown in Fig. 2, the ΔT in the 2D case yield the same values as the 1D geometry for $A \approx 100$ mm^2). In any case, for low values of A (narrow beams) the temperature differences between the 1D and 2D solutions are large even at early times ($t < L^2/\alpha \approx 7$ s). A direct comparison between the temperature increments predicted by the 2D model and experimental measurements will be shown later.

In order to compare the temperature increments given by Eq. (18) with other models, we revised the theoretical results of Lax [25], who considered a similar setup (semi-transparent material irradiated by a Gaussian beam), except that his formulation takes into account a semi-infinite z-coordinate and no convection occurs at the surface.

The maximum steady temperature increment θ_{max}, occurring at (r=0, z=0), was found by Lax [25] to be:

$$\theta_{max} = \frac{P_o}{2\pi^{1/2} kw}\left[w\beta\mathscr{D}(w\beta/2) - \frac{w\beta}{2\pi^{1/2}} exp\left(-w^2\beta^2/2\right) Ei\left(w^2\beta^2/2\right)\right] \quad (23)$$

where $\mathscr{D}$ denotes the Dawson's integral . Fig. 3a and b shows the ratio of the temperature increments given by Eq. (18) at (r=0,z=0,t=1000 s) and those given by Eq. (23) for different h_1/h_2 ratios and optical lengths, respectively. Fig. 3a shows that our results approximate Lax's solution as the heat transfer coefficient on the back surface of the membrane, h_2, becomes higher than the heat transfer at the front surface, h_1, i.e., when Eq. (18) favors heat flux towards the rear end, similar to the semi-infinite z approach. Interestingly, the θ_{max} found by Lax and those calculated using Eq. (18) do not differ more than 35% for five orders of magnitude of h_1/h_2. Fig. 3b shows the θ_{max} ratios now for different values of the optical length. Again, our results approach Lax's solution in the semi-infinite axial approach, which is achieved when the optical depth is larger than one.

3. Experimental setup

The polymer-carbon membranes were fabricated by mixing 2.3 mg/g of carbon nanopowder (<50 nm, Sigma Aldrich 633100) in

poly-dimethylsiloxane, PDMS, using a 1:10 ratio of polymer to curing agent. The composite was mixed by hand until an average carbon cluster size of about 30 μm was obtained, as determined through image processing of a magnified picture conducted in Matlab. The mixture was then poured in square molds made with coverslips (base) and mica sheets (lateral walls) and the thickness of the resulting membranes was subsequently measured with a micrometer. Different mica layers were simply added on top of each other in order to change the thickness L. Finally, the mixture was left to cure for 2 h at 75 °C. Fig. 4a shows some membranes having different thicknesses L, from 137 to 550 μm. The thickness of the membranes becomes evident observing the different gray scale of the pictures. A reference membrane (L=155 μm) was also fabricated using only PDMS. The amount of carbon added to the PDMS (0.23%) is not expected to increase the thermal conductivity of the polymer; therefore, the thermal properties of the composite were considered to be the same as for pure PDMS: ρ=965 Kg/m^3, k = 0.2 W/m·K, C_p = 1460 J/Kg·K and $\alpha = k/C_p\rho$ = 0.1419 mm^2/s [28]. Note that in our experiments, the optical depth, $\tau_\lambda=\beta L$, is changed by varying the thickness L of the membranes. In principle, it is also possible to vary τ_λ by changing the concentration of the photo-absorbing particles while fixing the value of L, as it was done in Ref. [29].

For the temperature measurements, the membranes were put in contact with a resistive temperature sensor (TH100PT, Thorlabs), see Fig. 4b. In most of the measurements, the coverslips were used as supports for the membranes. A thin layer of thermal paste was also used to ensure thermal contact between the membrane and the sensor. At the other side of the membrane (front surface), a laser diode (λ=975 nm, 200 mW maximum output power) coupled to an optical fiber (Corning SMF-28e, NA = 0.14) was placed at a fixed distance of 1.7 mm. Since the beam coming from the optical fiber was not collimated nor focused, a fixed distance between the fiber and the membrane yields a uniform irradiated area in all the measurements. Using the angle of acceptance of the optical fiber, $sin^{-1}(NA)$, we estimated a spot radius of w=158 μm. Thus the parameter A=12.5×10^{-3} mm^2 in all cases. Also, to ensure a single-mode output with a gaussian intensity profile, a mode stripper was used near the output end of the optical fiber.

The extinction coefficient was determined according to the Beer–Lambert law $\beta=-(1/L)ln(I/I_o)$, where I_o is the input intensity at the membrane. For these measurements, the output beam coming from the fiber was collimated (FiberPort Collimator, Thor-Labs, spot size of 0.38 mm) and directed to the membranes, from which the transmitted intensity was registered subsequently using a photodetector (ILX Lightwave Optical Multimeter). Fig. 5 shows the extinction coefficients as a function of the optical intensity for different values of L.

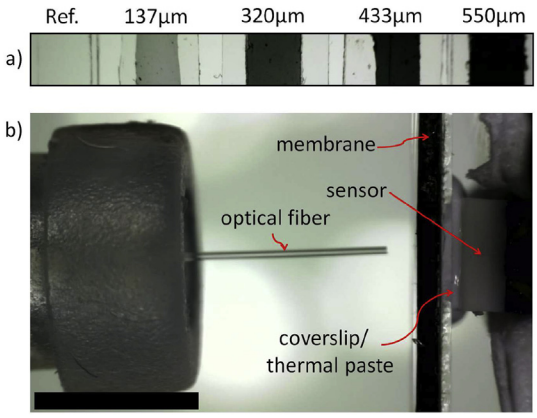

Fig. 4. Experimental setup. a) Pictures of some polymer-carbon membranes having different thickness L. Ref. denotes the reference membrane having no carbon nano-powder. b) Experimental setup used to measure the temperature increment in the back side of the membrane, the scale bar is 2 mm.

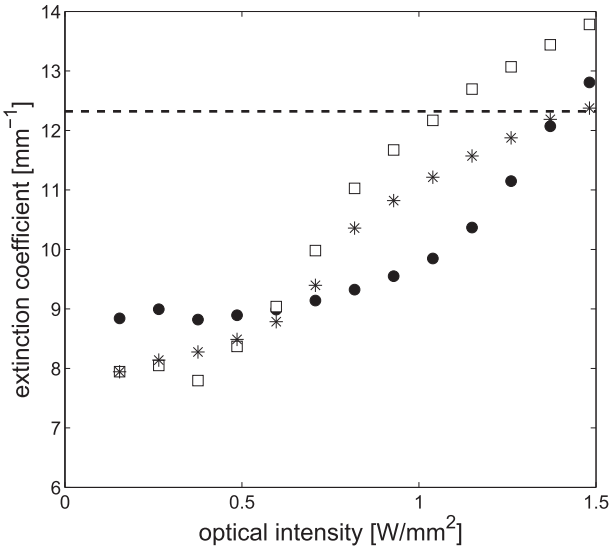

Fig. 5. Extinction coefficient of the membranes as a function of the optical intensity. The extinction coefficient was calculated according to $\beta=-(1/L)ln(I/I_o)$; (•) L=359.8 μm, (□) 405.2 μm, (*) 610.2 μm. The vertical dashed line denotes the absorption coefficient for carbon black clouds according to Bertocchi et al. [35].

The plots in Fig. 5 clearly show an increase of the extinction coefficient with the optical intensity. In accordance with previous reports [17–19], this increase of $\beta=\beta_{abs}+\beta_{scat}$ is linked to an increase in the scattering coefficient rather than in the absorption term. We therefore considered a basal absorption coefficient of ~8 mm^{-1} for our membranes. The horizontal dotted line denotes the absorption coefficient measured for carbon black clouds [35] using the same carbon concentration employed in the present work. This roughly supports the accepted idea that the optical properties of carbon black dispersions in air are similar to carbon dispersion in liquids [19]; evidently, in our case, the carbon is dispersed in a polymeric transparent matrix. For comparison, the absorption coefficient reported for carbon nanohorn suspensions [36] is about twice as those reported for carbon black clouds.

4. Results

The steady temperature as a function of the optical intensity for different membrane thicknesses L (137–550 μm) is shown in Fig. 6a. The dashed line indicates the temperature increment in the reference membrane, showing that the sensor has some response to light excitation. Nevertheless, this response is well below the data for the active membranes and should actually decrease as the thickness of the membranes increases. For the active membranes having 0.23% of carbon nanopowder, the temperature increases linearly with the optical intensity up to I_o~5 W/mm^2. This linear relationship at low temperatures has also been observed, for example, in skin phantoms induced by pulsed lasers [37]. Such a behavior implies two important features of the membranes. Firstly, the thermal properties of the composite seem to behave as constants for the observed temperature range; secondly, even though the composite already experiments nonlinear scattering at these optical intensities (see Fig. 5), the scattering contribution does not seems to alter the absorption and the steady temperature trend. Above 5 W/mm^2, the points deviate from the linear behavior as I_o increases. This broadly coincides with the appearance of

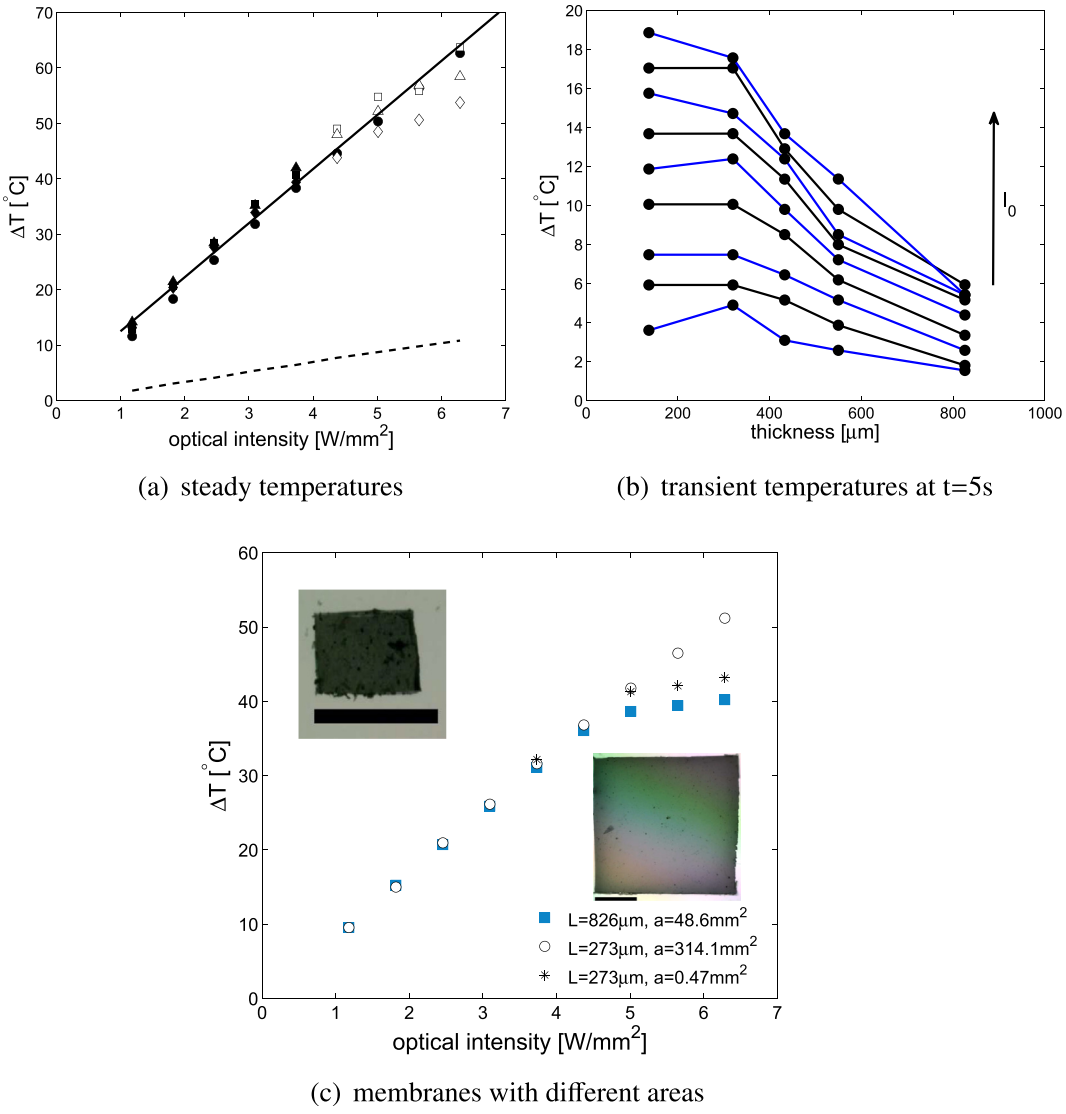

(a) steady temperatures

(b) transient temperatures at t=5s

(c) membranes with different areas

Fig. 6. Experimental temperature increments measured at the back surface of the membranes. a) Steady temperatures as a fuction of the optical intensity for different values of L: (•) 137 μm, (■) 320 μm, (▲) 433 μm, (◆) 550 μm. The empty symbols denote those cases where incandescence at the front side was observed. The dashed line corresponds to the reference membrane having no carbon nanopowder; the solid line is a linear fitting for all data for I_o<5 W/mm^2. b) ΔT as a function of L measured 5 s after turning on the laser diode. The different lines correspond to different optical intensities whose range was 1.18–6.29 W/mm^2 in 0.638 increments. c) ΔT as a function I_o for different values of L and membrane area a. The insets show two membranes cut with different sizes: the top-left image corresponds to a=0.47 mm^2, the scale bar is 1 mm; bottom-right image corresponds to a=314.1 mm^2, the scale bar is 5 mm.

incandescence at the front side of the membranes, occurring at optical intensities denoted by empty symbols in Fig. 6a. The temperature deficit at the back surface is therefore a consequence of the emission at the front surface, and it is stronger as the thickness L increases because less heat diffuses towards these regions. Interestingly, in the conduction regime (1–5 W/mm^2), the steady temperature does not change significantly with the parameter L. Note that at the hypothetical limit $\beta \to \infty$, the temperature at the back of the membrane should decrease as a function of L, as expected for a pure conduction regime. In the discussion section we will use Eq. (18) to show that in semitransparent materials, a $\Delta T = f(L,\beta)$ plot reveals conditions where ΔT strongly depends on L and β variations, and others where ΔT acquires a stationary or maximum value (low dependance on L).

It is worthwhile mentioning that samples prepared following different procedures were also tested for heat generation (data not shown). As an example, when the nanopowder was dispersed in the polymer using organic solvents (e.g., chloroform) and/or mechanical mixers, the resulting increase in temperature was comparatively lower than the one reported above. We also observed that aging of the mixture has some hindering effects on ΔT. These observations highlight the importance that the microstructure or size of the dispersed phase has on the heat generation capacity of the membranes, as reported for other kinds of composites [38]. It is therefore evident that the degree of clustering (cluster size) of the carbon nanoparticles constitute another important factor that has to be studied regarding the heat generation capacity of these composites; in general terms, it is expected that as the cluster size increases, the heat generated in the membrane will be larger.

Fig. 6b presents now the ΔT as a function of the membrane thickness 5 s after turning on the laser diode (transient regime). As expected, more heat propagates along thinner membranes since these yield shorter characteristic times $t \approx L^2/\alpha$. Hence, even though

the steady state temperature does not vary significantly for different values of L, regardless the time required to reach the stationary value, the transient temperature does vary with the thickness L. This implies that an optimum membrane thickness is expected to deliver a maximum heat in the transient regime (for L=0, of course, no heat generation occurs).

Possible effects on ΔT due to the membrane area (i.e., sample size) were also evaluated. This was done for membranes having different thicknesses and areas ranging from 0.47 to 314.1 mm^2 (see Fig. 6c). Surprisingly, all the tested membranes achieved the same ΔT regardless its size and depth. This behavior suggest that heat generation is indeed very localized, as it should be given that the radiation is delivered by an optical fiber. It is reasonable to think that the effects of the membrane area a on ΔT will only be seen for the cases when a approach the area of the laser spot (0.18 mm^2 in our case), which corresponds to a square membrane having a size of just ~0.5 mm. In future experiments we plan to measure the temperatures on the membranes with smaller sensors in order to determine, in a more "punctual" manner, temperature differences with respect to the membrane dimensions. Finally, note that for I_0>5 W/mm^2, Fig. 6c shows again a departure from the linear response due to heat losses at the surface, as discussed above.

5. Discussion

The comparison between the experimental and theoretical ΔT values has its own limitations mainly because the exact values for some parameters are unknown. In particular, the sensor-membrane interface involves several media making difficult to specify the global heat transfer coefficient h_2. Also, since the sensor size is of the order of the membrane area but much larger than the irradiated area, the measured ΔT do not constitute punctual temperatures but rather mean temperatures. Nonetheless, it is of course illustrative to compare both data and verify if the 2D axi-symmetric solution is able to represent the experimental results. As a case of study, we chose the temperature data obtained with a membrane having L=826 μm. For this experiment, we removed the coverslip in order to avoid a layered composite on one side of the membrane. This allows for adjusting only one convection parameter for the membrane-sensor interface. Without the glass coverslip, the registered increase in temperature was 14–20% higher than those obtained in the previous experiments.

The fitting procedure of Eq. (18) to the experimental data was done as follows: first, we fed the equation with all the known parameters: I_o, k, α, A, h_1 (convection in air), and adjusted h_2 to fit the steady temperature values. This initial adjustment was done for the lowest I_o tested in the experiments (1.18 W/mm^2, see ∘ symbols in Fig. 7). The value of β was chosen to be 8 mm^{-1} since the results suggested that scattering plays a minor role in the steady temperature. Subsequently, the value of the thermal diffusivity α was also adjusted to match the experimental characteristic time required to reach the steady state. For the results shown in Fig. 7, Eq. (18) fits the experimental data for $h_2 = 2000$ W/m^2·K and α=0.01 mm^2/s, the latter being one order of magnitude lower than the theoretical value (i.e., α for pure PDMS). After these initial adjustments in h_2 and α, all the other theoretical curves fit quite well the corresponding experimental points, as can be seen in Fig. 7. Furthermore, even for the cases in which the nonlinear scattering effects were present, their influence were taken into account by the fitting parameters α or h_2. Note however that Eq. (18) fails to fit the highest optical intensity data (◆ symbols in Fig. 7): this reflects the limitation of the present model since it does not consider emission and/or strong scattering effects seen experimentally at high I_o values.

Now, there can be two reasons why the effective value of the thermal diffusivity was found to be one order of magnitude lower than the theoretical one. As mentioned in the introduction, light scattering presumably has small effects on the steady state; however, it can play a relevant role during the transient period slowing down the rise in temperature. It is a fact, after Fig. 5, that the composite membranes have nonlinear scattering effects, so this may be a plausible explanation for such heat transfer retardation. The other reason for observing low values of α could be a matter of the experimental setup or the structure of the composite. During the determination of α with laser flash techniques, Always-Cooper & coauthors [39] realized that apparent diffusivities can be created if additional thermal resistances inherent to the setup are not taken into account. In our case, additional resistance contributions may arise from the sensor or from the interface between the carbon and the polymer. In other similar studies it has been found, for instance, that the effective thermal conductivity, and therefore the thermal diffusivity, depends on the size of the "fillers" mixed with the polymeric matrix [38]. In our case the carbon nanotubes form "islands" or clusters due to the way they were dispersed, it is therefore probable that such microstructure will reduce the effective thermal diffusivity as consequence. Thus far we are unable to determine which is the dominant effect on α and further experiments are needed in this regard.

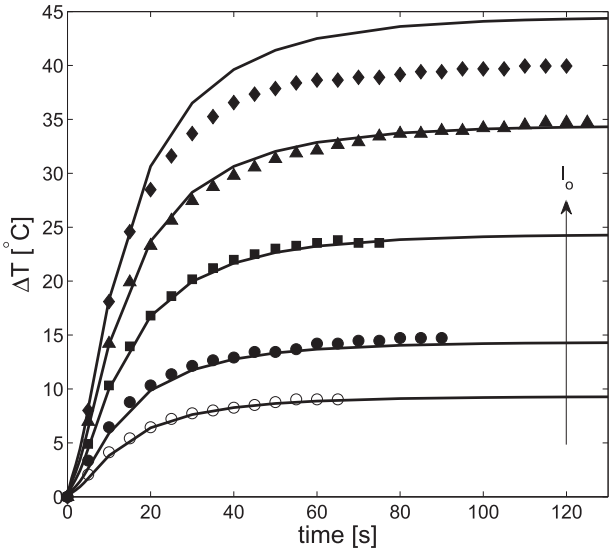

Fig. 7. Comparison of the unsteady theoretical and experimental temperature increments. Symbols: experimental values for different optical intensities, (∘) 1.18 W/mm^2, (•) 1.82 W/mm^2, (■) 3.09 W/mm^2, (▲) 4.37 W/mm^2, (◆) 5.65 W/mm^2. Solid lines: theoretical values; L=826 μm, $h_1 = 10$ W/m^2·K, $h_2 = 2000$ W/m^2·K, $k = 0.2$ W/m·K, α=0.01 mm^2/s, β=8 mm^{-1}, A=12.5×10^{-3} mm^2.

5.1. Effect of β and L on the temperature ΔT

As shown in Fig. 6a, the steady state temperature was not affected by the membrane thickness L in a significant way. In the following we will see that Eq. (18) can reproduce this experimental behavior; in fact, Eq. (18) yields in general L–ΔT plots that exhibit stationary values (maximum points) for a given value of β. Using the thermal properties determined in the last section, we plotted the theoretical ΔT at the back side of the membranes as a function of L and β. The curves are displayed in Fig. 8. We can see that an increase in β not only increases the values of ΔT but also changes the tendency of $\Delta T|_{z=L}$ as a function of L. For very small values of β (0.01 mm^{-1}, blue dashed line in Fig. 8) higher temperatures are achieved as L increases due to the increase of the optical depth $\tau_\lambda = \beta L$. Conversely, in the limit when $\beta \to \infty$, where the optical thick

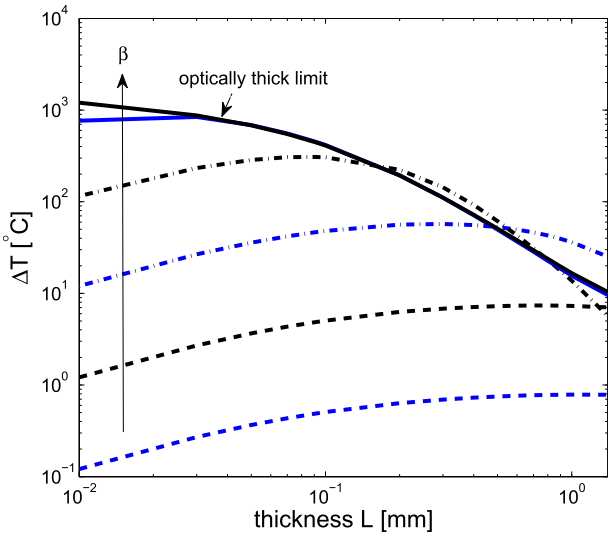

Fig. 8. Theoretical ΔT values at (r=0, z=L) as a function of L for different values of β. The thermal properties are the same as those mentioned in Fig. 7 for the specific case of I_o=3.09 W/mm^2, t = 1 min. The lines from bottom to top represent different values of β: 0.01, 0.1, 1, 10, 100 and 1000 mm^{-1}.

limit is achieved, $\tau_\lambda \to \infty$ and ΔT decreases with the parameter L. Fig. 8 then suggest that every L–ΔT curve has a maximum or stationary point at an optimal value L_{op}; this optimal point in turn reduces as β increases. Therefore, for membranes whose thicknesses fall near the optimal L–ΔT point, Eq. (18) predicts that ΔT will be a slow varying function with respect to L. This is what we actually observed in the experiments, where the steady temperature has low variations with respect to L but at the same time has a maximum at L~433 μm. Similar curves have been observed in materials with significant scattering effects. In those cases, it is the radiative heat flux the one that exhibits a maximum value at a L_{op} given certain absorption and scattering coefficients [30].

5.2. Radial temperature profiles

We finish the discussion by presenting the theoretical radial profiles of ΔT in the membranes. Fig. 9a presents $\Delta T|_{z=L}$ as a function of the radial distance. The symbols correspond to the values obtained by numerical integration of Eq. (14) using z=L for different times. The solid line is the steady value obtained with the delta approximation, Eq. (22). Clearly, the numerical values at t=1000 s (◆ symbols in Fig. 9) are in very good agreement with Eq. (22), indicating that the delta approximation is valid for small values of A, in our case obtained experimentally with an optical fiber. Note that 80% of the maximum temperature decays within r=1 mm. Eq. (22) is also useful to obtain the steady state temperature contours in the z–r plane, an example is depicted in Fig. 9b. For regions confined in the zone (z<0.3, r<0.2 mm), the temperature increases unrealistically due to the Bessel function $\mathscr{K}_0$ in Eq. (22). Nonetheless, for these cases, Eq. (18) can be used as a complement to compute ΔT at z=r=0; i.e., the maximum temperature increment, which for this case corresponds to 714 °C (I_o=3.09 W/mm^2). For comparison, pure multi-walled carbon nanotubes in vacuum can reach temperatures up to ~2500 K. It is expected that the polymer molecules exposed to such temperatures will decompose on the surface. While this is unfavorable for the performance of the membranes as heat delivers in the long term (lower powers will be necessary to avoid evaporation or decomposition of the surrounding matrix), this condition has been actually used to etch micropatterns in PDMS surfaces [10].

6. Conclusions

In this work we measured the temperature increase in PDMS-carbon nanopowder membranes upon light irradiation with an optical fiber. Maximum temperature increments ΔT, measured at the back surface of the membranes (front surface is the one facing the optical fiber tip), were around ~50 °C, following a linear dependance with the optical intensity I_o. For higher I_o, the temperatures reached ~65 °C, although at these optical powers the composite surface experienced incandescence and the heat conduction regime (linear) is lost due to emission or strong scattering effects. Besides the temperature measurements, we also determined the extinction coefficient β in the membranes by measuring the transmitted light with a photodetector. The I_o–β curves revealed a nonlinear scattering behavior of the composites, as is commonly observed in carbon allotropes dispersions. Surprisingly, the increase of the scattering contribution did not alter the

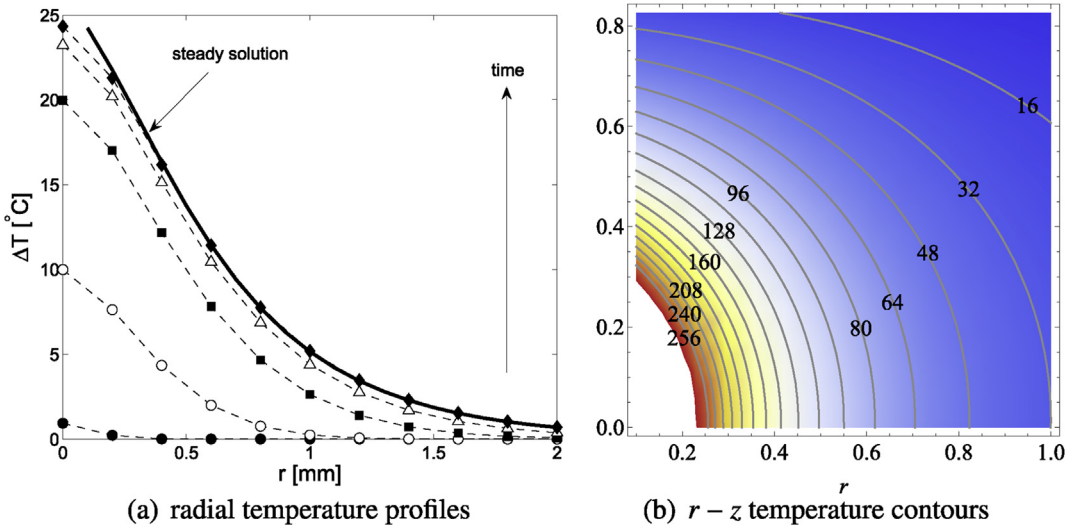

Fig. 9. Radial temperature profiles as predicted with the delta approximation Eq. (22). The thermal properties are the same as those used in Fig. 7 for the specific case of I_o=3.09 W/mm^2. a) solid line: theoretical values estimated with Eq. (22); symbols denote the values obtained by numerical integration of Eq. (14) at different times: (•) t = 1s, (◦) 10s, (■) 30s, (△) 60s, (◆) 1000 s b) ΔT contours in the z–r plane obtained with Eq. (22). The numbers in the figure correspond to the temperatures ΔT[°C], z and r are in millimeters.

expected linear response of the steady ΔT as a function of I_o. The temperature values were also compared for different membrane thicknesses L. All the steady state measurements resulted in similar ΔT regardless the values of L; however, the transient response was found to be dependent on L. This is an expected behavior since the characteristic heat time scales with L^2/α.

The experimental data was also analyzed with a theoretical framework using the Green's function formulation. We obtained two analytical formulas for heat conduction in cylindrical coordinates that emulate the heat flux in a membrane surrounded by dissipating media (boundary conditions defined by two heat transfer coefficients). The theoretical solution was capable to fit the transient experimental data, $t-\Delta T$ plots, only when the thermal diffusivity was one order of magnitude lower than the expected value for PDMS (from 0.142 to 0.01 mm^2/s). We concluded that this can be due either to the nonlinear scattering behavior of the material (supporting the hypothesis that scattering does not affect the steady state but alters the transient response), or due to additional thermal resistances imposed by the experimental setup.

Another important aspect of the experimental and theoretical results is that the $L-\Delta T$ curves, temperature as a function of the membrane thickness, showed a maximum point at an optimum value of L, which is in turn a function of the extinction coefficient β. Finally, the results also showed that similar steady state temperature increments ΔT were achieved regardless the size (area) of the membranes, provided that the illuminated area, which was of the order of 0.2 mm^2, is smaller than the membrane area. This suggested that the heat generation produced by the optical fiber is indeed very localized; the theory also supports this observation since the numerical steady solutions were almost identical to one analytical solution found by approximating the Gaussian beam with the delta function.

It is our hope that the results of the present investigation could be used to design composite membranes as heat deliverers. The thickness L constitutes one of the critical design parameters and can be selected in order to deliver the maximum ΔT (L_{op}) or yield small response times. Another important parameter that should be studied with more detail in the future is the size of the nanoparticle clusters. In this regard we can distinguish two limiting regimes: if the particles are well dispersed (no clustering), the mixture will have better thermal conductivity characteristics but poor heat generation capabilities (good conduction, poor generation); on the other hand, if the particles are dispersed in such a way to promote clustering, the mixture will acquire a minor improvement of the thermal conductivity characteristics but will achieve good heat generation capabilities (poor conduction, good generation). In between these two regimes we would find bi-dispersed regimes that will share both characteristics, i.e., have good thermal conductivity as well as good heat generation capacities.

Acknowledgments

The authors appreciate the financial support from Conacyt-México under grant 154464. We also acknowledge the useful suggestions made by Dr. Luke W. Sciberras in the theoretical calculations. R. Vélez-Cordero appreciate as well the financial support of Cátedras-CONACyT.

References

[1] Z.H. Lim, A. Lee, Y. Zhu, K.-Y. Lim, C.-H. Sow, Sustained laser induced incandescence in carbon nanotubes for rapid localized heating, Appl. Phys. Lett. 94 (2009) 073106 1–3.
[2] K. Mizuno, J. Ishii, H. Kishida, Y. Hayamizu, S. Yasuda, D.N. Futaba, M. Yumura, K. Hata, A black body absorber from vertically aligned single-walled carbon nanotubes, PNAS 106 (2009) 60446047.
[3] A.K. Geim, K.S. Novoselov, The rise of graphene, Nat. Mat. 6 (2007) 183191.
[4] S. Berber, Y.-K. Kwon, D. Tománek, Unusually high thermal conductivity of carbon nanotubes, Phys. Rev. Lett. 84 (2000) 46134616.
[5] R. Tilley, Colour and the Optical Properties of Materials, John Wiley & Sons, GB, 2000.
[6] S.-i. Tanaka, M. Matsunami, S.-i. Kimura, An investigation of electron-phonon coupling via phonon dispersion measurements in graphite using angle-resolved photoelectron spectroscopy, Nat. S. Rep. 3 (2013) 3031 1–6.
[7] P. Avouris, M. Freitag, V. Perebeinos, Carbon-nanotube photonics and optoelectronics, Nat. Photonics 2 (2008) 341–350.
[8] T. Kampfrath, L. Perfetti, F. Schapper, C. Frischkorn, M. Wolf, Strongly coupled optical phonons in the ultrafast dynamics of the electronic energy and current relaxation in graphite, Phys. Rev. Lett. 95 (2005) 187403 1–4.
[9] J.W. Fisher, S. Sarkar, C.F. Buchanan, C.S. Szot, J. Whitney, H.C. Hatcher, S.V. Torti, C.G. Rylander, M.N. Rylander, Photothermal response of human and murine cancer cells to multiwalled carbon nanotubes after laser irradiation, Cancer Res. 70 (2010) 9855–9864.
[10] M. Hautefeuille, L. Cabriales, R. Pimentel-Domínguez, V. Velázquez, J. Hernández-Cordero, L. Oropeza-Ramos, M. Rivera, M.P. Carreón-Castro, M. Grether, E. López-Moreno, New perspectives for direct PDMS microfabrication using a CD-DVD laser, Lab. Chip 13 (2013) 4848–4854.
[11] J.R. Vélez-Cordero, A.M. Velázquez-Benítez, J. Hernández-Cordero, Thermocapillary flow in glass tubes coated with photoresponsive layers, Langmuir 30 (2014) 5326–5336.
[12] M. Nour, K. Berean, S. Balendhran, J. Zhen Ou, J. Du Plessis, C. McSweeney, M. Bhaskaran, S. Sriram, K. Kalantar-zadeh, CNT/PDMS composite membranes for H2 and CH4 gas separation, Int. J. Hydrog. Energ. 38 (2013) 10494–10501.
[13] Z. Han, A. Fina, Thermal conductivity of carbon nanotubes and their polymer nanocomposites: a review, Prog. Polym. Sci. 36 (2011) 914944.
[14] S. Wu, W.-T. Liu, X. Liang, P.J. Schuck, F. Wang, Y.R. Shen, M. Salmeron, Hot phonon dynamics in graphene, Nano Lett. 12 (2012) 5495–5499.
[15] C.-W. Nan, R. Birringer, D.R. Clarke, H. Gleiter, Effective thermal conductivity of particulate composites with interfacial thermal resistance, J. Appl. Phys. 81 (1997) 6692–6699.
[16] A.M. Marconnet, N. Yamamoto, M.A. Panzer, B.L. Wardle, K.E. Goodson, Thermal conduction in aligned carbon nanotube polymer nanocomposites with high packing density, ACS Nano 5 (2011) 48184825.
[17] J. Wang, Y. Chen, R. Li, H. Dong, L. Zhang, M. Lotya, J.N. Coleman, W.J. Blau, Nonlinear optical properties of graphene and carbon nanotube composites, in: Siva Yellampalli (Ed.), Carbon Nanotubes – Synthesis, Characterization, Applications, InTech, 2011, ISBN 978-953-307-497-9. Available from: http://www.intechopen.com/books/carbon-nanotubes-synthesis-characterizationapplications/nonlinear-optical-properties-of-graphene-and-carbon-nanotube-composites.
[18] P. Chen, X. Wu, X. Sun, J. Lin, W. Ji, K.L. Tan, Electronic structure and optical limiting behavior of carbon nanotubes, Phys. Rev. Lett. 82 (1999) 25482551.
[19] K. Mansour, M.J. Soileau, E.W. Van Stryland, Nonlinear optical properties of carbon-black suspensions (ink), J. Opt. Soc. Am. B 9 (1992) 1100–1109.
[20] S. Maity, J.R. Bochinski, L.I. Clarke, Metal nanoparticles acting as light-activated heating elements within composite materials, Adv. Funct. Mater. 22 (2012) 5259–5270.
[21] K. Boubaker, Temperature profile distortion due to radiative effects beneath graphite-coated plate steel sample heated by Gaussian beam, Eur. Phys. J. Appl. Phys. 28 (2004) 249–253.
[22] M. Lazard, S. André, D. Maillet, Diffusivity measurement of semi-transpatent media: model of the coupled transient heat transfer and experiments on glass, silica glass and zinc selenide, Int. J. Heat Mass Transfer 47 (2004) 277–487.
[23] J.C. Kneip, B. Martin, A. Loredo, S. Mattei, D. Grevey, Heat transfer in semi-transparent materials during laser interaction, J. Matter. Process. Tech. 155–156 (2004) 1805–1809.
[24] H.-L. Yi, M. Xie, H.-P. Tan, Transient coupled heat transfer in an anisotropic scattering composite slab with semitransparent surfaces, Int. J. Heat Mass Transfer 51 (2008) 5918–5930.
[25] M. Lax, Temperature rise induced by a laser beam, J. Appl. Phys. 48 (1977) 3919–3924.
[26] E. Abraham, J.M. Halley, Some calculations of temperature profiles in thin films with laser heating, Appl. Phys. A 42 (1987) 279–285.
[27] B.C.H. Wendlandt, Temperature in an irradiated thermally conducting translucent medium, J. Phys. D. Appl. Phys. 6 (1973) 657–660.
[28] I.K. Tjahjono, Y. Bayazitoglu, Near-infrared light heating of a slab by embedded nanoparticles, Int. J. Heat. Mass Transfer 51 (2008) 15051515.
[29] J. Vera, Y. Bayazitoglu, Gold nanoshell density variation with laser power for induced hyperthermia, Int. J. Heat Mass Tran 52 (2009) 564573.
[30] J. Vera, Y. Bayazitoglu, A note on laser penetration in nanoshell deposited tissue, Int. J. Heat Mass Transfer 52 (2009) 34023406.
[31] M.F. Modest, Radiative Heat Transfer, 3th edition, Academic Press, USA, 2013.
[32] D.W. Hahn, M.N. Oẓişik, Heat Conduction, 3th edition, John Wiley & Sons, USA, 2012.
[33] P. Majumdar, H. Xia, A Green's function model for the analysis of laser heating of materials, Appl. Math. Model 31 (2007) 1186–1200.
[34] I.S. Gradshteyn, I.M. Ryzhik, A. Jeffrey, Table of Integrals, Series and Products, fifth ed., Academic Press, USA, 1994.

[35] R. Bertocchi, A. Kribus, J. Karni, Experimentally determined optical properties of a polydisperse carbon black cloud for a solar particle receiver, J. Sol. Energy-T ASME 126 (2004) 833–841.
[36] L. Mercatelli, E. Sani, G. Zaccanti, F. Martelli, P.D. Ninni, S. Barison, C. Pagura, F. Agresti, D. Jafrancesco, Absorption and scattering properties of carbon nanohorn-based nanofluids for direct sunlight absorbers, Nanoscale Res. Lett. 6 (282) (2011) 1–9.
[37] F. Sun, A. Chaney, R. Anderson, G. Aguilar, Thermal modeling and experimental validation of human hair and skin heated by broadband light, Laser Surg. Med. 41 (2009) 161–169.
[38] P. Yi, R.A. Awang, W.S.T. Rowe, K. Kalantar-zadeh, K. Khoshmanesh, PDMS nanocomposites for heat transfer enhancement in microfluidic platforms, Lab. Chip 14 (2014) 3419–3426.
[39] R.M. Alway-Cooper, M. Theodore, D.P. Anderson, A.A. Ogale, Transient heat flow in unidirectional fiber-polymer composites during laserssss flash analysis: experimental measurements and finite element modeling, J. Compos. Mater. 47 (2013) 2399–2411.